Chapter 4

Discussions

In the previous work by Laongjit (M.S.Thesis, 2004), the oxalato complexes were prepared by mixing aqueous solutions of $K_3[Cr(C_2O_4)_3].3H_2O$, $K_3[Al(C_2O_4)_3].3H_2O$, and NaCl at room temperature. Three types of crystals were obtained, two were dark red almost black and the other was blue. They were designated as RedCubic, RedHexagonal, and Blue and characterized by scanning electron microanalysis/ energy dispersive X-ray fluorescence (SEM/EDX), inductively-coupled plasma/atomic emission spectroscopy (ICP-AES), single crystal X-ray diffraction, UV-Visible absorption spectroscopy (UV-Vis), fourier-transformed infrared spectrometry (FT-IR), X-ray powder diffraction (XRD), thermogravimetry analyzer (TGA), and differential scanning calorimeter (DSC). Crystal structure of RedHexagonal were studied by single crystal X-ray diffraction. The crystal structure of RedHexagonal could be solved but not for the RedCubic and Blue. The substitution of Cr^{3+} in $[Al(C_2O_4)_3]^{3-}$ yielded the complex $K_{18}\{K[Al_{0.97}Cr_{0.03}(C_2O_4)_3]_6\}Cl.18H_2O$ (RedHexagonal) which contained 3% of chromium. UV-Visible in aqueous solution was used to confirm d-d transition of Cr^{3+} (d^3) as three bands (298, 420, and 572 nm) were observed. The oxalate ligand exhibits one intense band at 298 nm which can be assigned to the $\pi \rightarrow \pi^*$ electronic transitions. Infrared spectroscopy was used to confirm the mode of vibrations of the oxalate ligands in the free state compared with that in the complexes. The C═O stretching of RedCubic, RedHexagonal, and Blue showed intense bands in the range 1723-1675 cm^{-1} whereas the C─O stretching modes showed intense bands in the range 1408-1271 cm^{-1}. The frequencies of the M─O frstretching modes appeared in the region 586-473 cm^{-1}. The results of TGA analysis of RedCubic, RedHexagonal, and Blue indicated that RedCubic lost 16.10%,

RedHexagonal 11.08%, and Blue 10.15% of weight in the range from room temperature to about 100°C which agreed with the results of DSC showing endothermic peak about 100°C assigned to the loss of water molecules in the structure.

In this work, the products were further studied with the other method for examples, UV-Vis in solid state (powder and crystalline),[13]C-NMR, EPMA, and density of complexes. Moreover, other products that prepared by the same method but with the varied amount of $K_3[Cr(C_2O_4)_3]\cdot 3H_2O$ were also characterized for the elemental composition by ICP-AES and WDXRF.

The preparation scheme in this work can be summarized as shown in Figure 31.

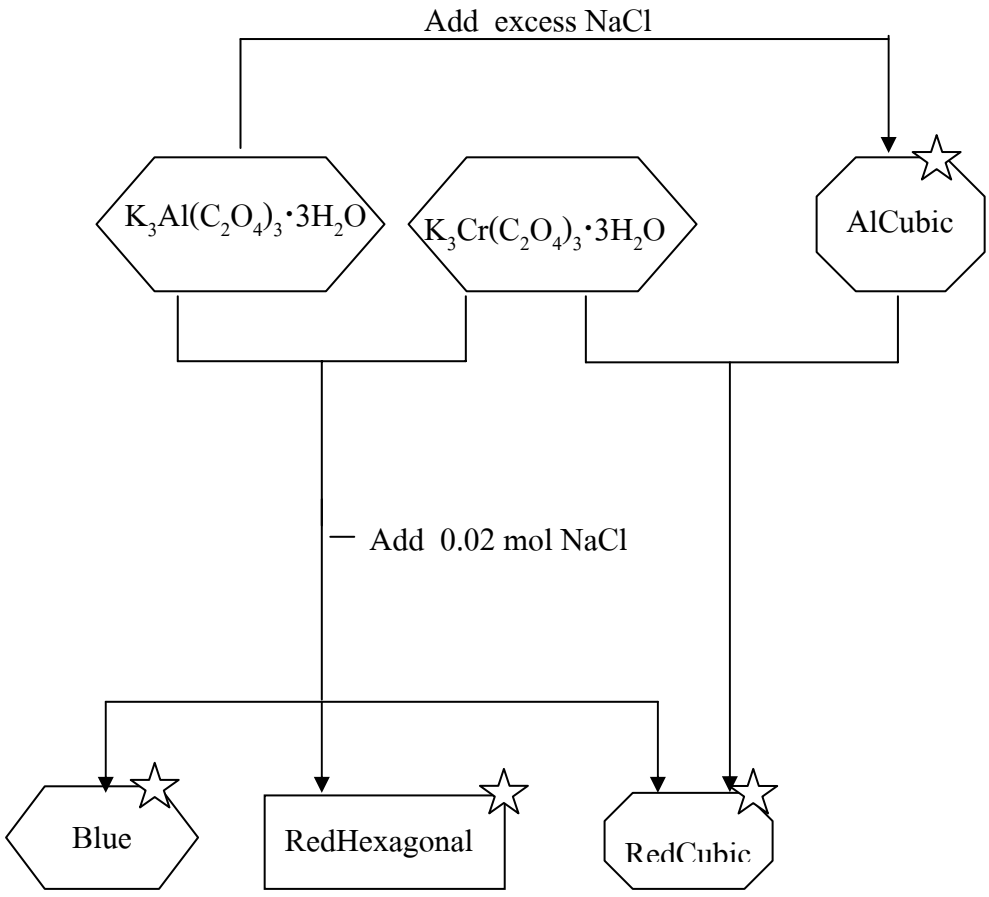

Figure 31 Preparation scheme for the doped Al-oxalato complexes

(☆ Products in this work)

Products from the mixing of $K_3Al(C_2O_4)_3 \cdot 3H_2O$, $K_3Cr(C_2O_4)_3 \cdot 3H_2O$ and NaCl consisted of RedCubic, RedHexagonal, and Blue while AlCubic was from $K_3Al(C_2O_4)_3 \cdot 3H_2O$ and NaCl. AlCubic was compared with RedCubic coresponding to elemental compositions are similar but only the color was different. The products (RedCubic, AlCubic, and Blue) were further studied with several methods such as by tritration technique for the amount of oxalate, by ICP-AES and EDXRF for other elemental compositions and by TGA for the water content in the complex. These data led to the general formula of the products as shown in Table 6 .

Table 6 Chemical formula of products and

Sample	Crystal system	Colour	General formula
$K_3Al(ox)_3 \cdot 3H_2O$	Monoclinic	colourless	$K_3Al(C_2O_4)_3 \cdot 3H_2O$ (Taylor, 1978)
$K_3Cr(ox)_3 \cdot 3H_2O$	Monoclinic	dark green	$K_3Cr(C_2O_4)_3 \cdot 3H_2O$ (Taylor, 1978)
Blue 5%	Monoclinic	blue	$K_3[Al_{0.95}Cr_{0.05}(C_2O_4)_3] \cdot 3H_2O$
RedHexagonal 5%	Hexagonal	reddish purple	$K_{18}\{K[Al_{0.97}Cr_{0.03}(C_2O_4)_3]_6\}Cl.18H_2O$ (Chaiyapoom, 2004)
RedCubic 5%	Cubic	reddish purple	$K\,Na_2[Al_{0.95}Cr_{0.05}(C_2O_4)_3] \cdot 4H_2O$
AlCubic	Cubic	colourless	$K\,Na_2[Al(C_2O_4)_3] \cdot 4H_2O$

Daniele (1983) studied the formation and stability of Li^+, Na^+, and K^+ complexes with oxalate by the potentiometric method at various ionic strengths. The results showed that the trend $K^+ > Na^+ > Li^+$, suggesting that weak complexes, according to an $Li^+ > Na^+ > K^+$ order, were formed.

Syntheses of the complexes of the $R_2[Mo_2O_5(C_2O_4)_2(H_2O)_2]$ type (R = K, Rb, Cs, NH_4, $N(CH_3)_4$), were reported in 1977 by Becher and coworker and their structures were speculated only on the basis of spectral data. According to these results, salts with the Rb^+ and NH_4^+ cations should contain anions with a linear symmetric Mo–O–Mo bridge, while for the Cs^+ and $[(CH_3)_4N]^+$ salts, they claimed that the bridge must be of a different kind. Such findings stimulated the structure determination of $[(CH_3)_4N]_2[Mo_2O_5(C_2O_4)_2(H_2O)_2]$ by Cindric´and coworker.They found that the bridge between two Mo atoms was of the Mo–O–Mo type with an angle of 177.6(2)° at the oxygen atom.(Cindric´ et al., 1999)

About the effect of size of cations, Na and K are 0.97 and 1.33 Å, respectively. Na is smaller than K so that it can displace in K position. And in general, as the cation decrease in size the lattice is stabilized (lattice energy becomes more negative) until anion-anion contact occurs(Huheey et al., 1993). Smaller cation can form complex more stable than larger cation, so RedCubic formed when mixed NaCl and size of cation may affect the structure.

Color formed in products when mixing $K_3Cr(ox)_3 \cdot 3H_2O$ with $K_3Al(ox)_3 \cdot 3H_2O$ may result from Cr ions inserting in complexes in resemblance to that occurs in ruby, (Cr impurity in α-Al_2O_3).

Generally, the formation of α-Al_2O_3 from the metastable aluminas, α- and δ-Al_2O_3, involves the conversion of cubic close packing of O^{2-} ions into stable hexagonal close packing, where the O atoms form hexagonally close-packed lattice; the Al atoms occupy octahedral sites between the O planes. (Patra et al., 2005) In ruby, Cr were inserted in Al position.

Cr^{3+} Gemstones

Ruby is one examples of gemstone that contains Cr impurity and its color is due to excitation of an electron from one d-orbital to another d-orbital on the same atom often times gives rise to absorption in the visible region of the spectrum. The Cr^{3+} ion in octahedral coordination is a very interesting example of this. Slight changes in its environment lead to changes in the splitting of the t_{2g} and e_g orbitals, which changes the color of the material. Hence, Cr^{3+} impurities are important in a number of gemstones. Samples of them are shown in Table 7.

Table 7 Properties of Cr^{3+} gemstones (www.chemistry.ohio-state.edu)

	Ruby	Alexandrite	Emerald
Host	Corundum Al_2O_3	Chrysoberyl $BeAl_2O_4$	Beryl $Be_3Al_2Si_6O_{18}$
t_{2g}- e_g Splitting	2.23 eV	2.17 eV	2.05 eV
	556 nm	563 nm	596 nm
	17985 cm^{-1}	17762 cm^{-1}	16778 cm^{-1}
Color	Red	Blue-Green (Day light) Red (Candle light)	Green

In each of the gemstones Cr^{3+} impurities substitute for Al^{3+} on an octahedral site as shown in Figure 32

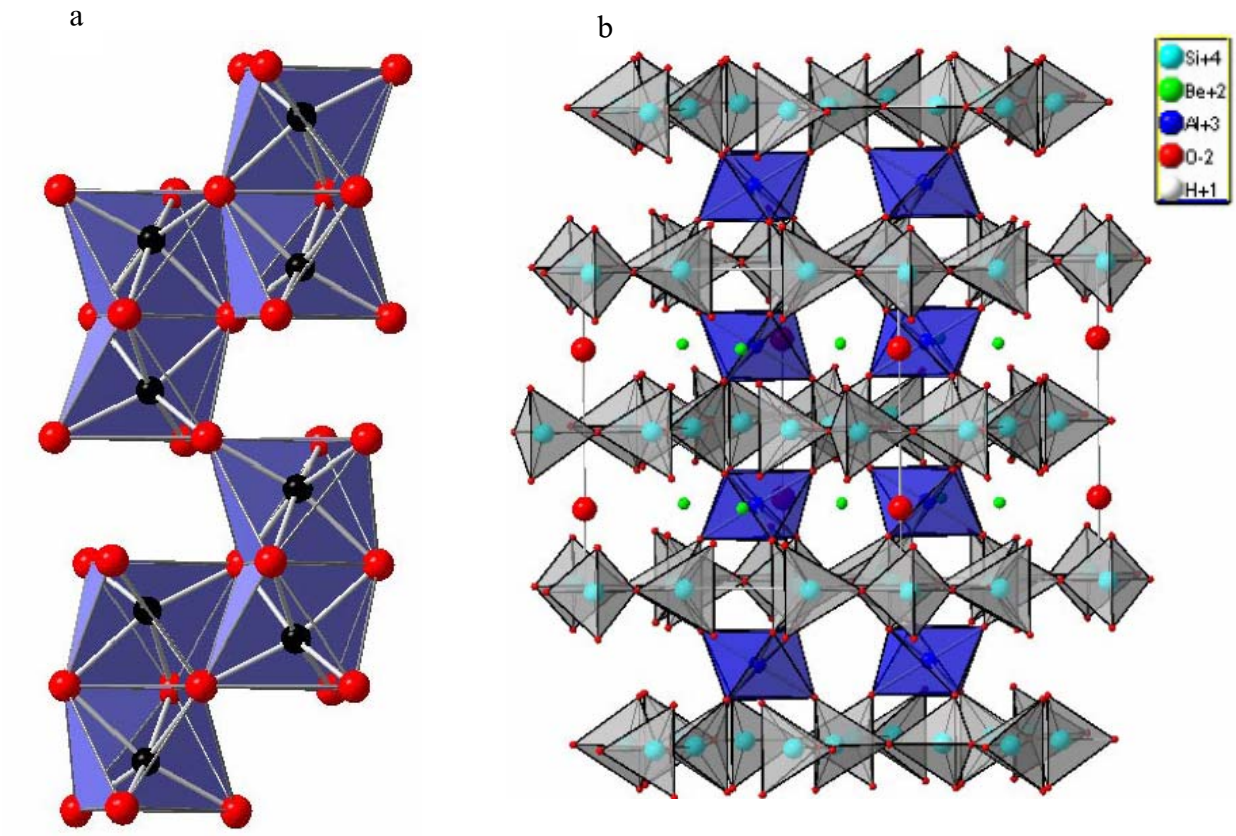

Figure 32 (a) Corundum, Al_2O_3, and (b) Beryl, $Be_3\ Al_2Si_6O_{18}$ (www.chemistry.ohio-state.edu)

The color in RedCubic, RedHexagonal, and Blue which change from colourless in $K_3Al(C_2O_4)_3 \cdot 3H_2O$ to one of each corresponding color is attributable to Cr ion inserted in the precursor structure similar to this gemstone.

4.1 Characterization of products

4.1.1 ^{13}C-NMR

In general ^{13}C-NMR is a valuable tool for observing rapid intramolecular rearrangement processes. The isotropic ^{13}C chemical shifts of the products have been measured at room temperature. A single signal that appear at the low magnetic field (~160-220 nm) are assigned to the carbons of the coordinated carboxylates. Suppose that the downfield shift corresponds to the decrease of the shielding effect in a diamagnetic contribution due to the decrease of the electron density on the carboxyl carbons.(Miessler and Tarr, 1998)

In this work, the ^{13}C-NMR spectra of RedCubic, RedHexagonal, and Blue display one single signal at the value of 167.023, 167.103, and 167.003 ppm, respectively, (Figures 10-12), intermediate between the single carbon signal occurring in free oxalic acid (163.16 ppm) and potassium oxalate (175.18 ppm). This spectral shape proves that the oxalato group acts as a bidentate ligand resulting in one single carbon enviroment. They indicate the equivalence of the two carbon atoms in oxalate implying the bidentate mode of binding to one metal ion. They show slightly different position due to the electron density on the carboxyl carbons.

In $K_3Al(C_2O_4)_3 \cdot 3H_2O$ complex, the δ values for carboxyl carbons from oxalate ligand bonding with Al (167.14 ppm) become greater (downfield shift) than the δ values for carboxyl carbons in free oxalic acid (163.16 ppm) because of the decrease of the electron density on the carboxyl carbons similar to that found in RedCubic, RedHexagonal, and Blue.

Boder et al. (2003) studies the $Al(C_2O_4)_{1-3}$ species by ^{13}C-NMR spestroscopy. The values of ^{13}C NMR shift of the detected binary species $Al(C_2O_4)_i^{+3-2i}$ are shown in Table 8. Three binary species are $Al(C_2O_4)^+$, $Al(C_2O_4)_2^-$, and $Al(C_2O_4)_3^{3-}$.The assignment of ^{13}C-NMR signals in the Al (III)- $(C_2O_4)^{2-}$-H^+ system can be done by varying the metal/ligand ratio and pH.

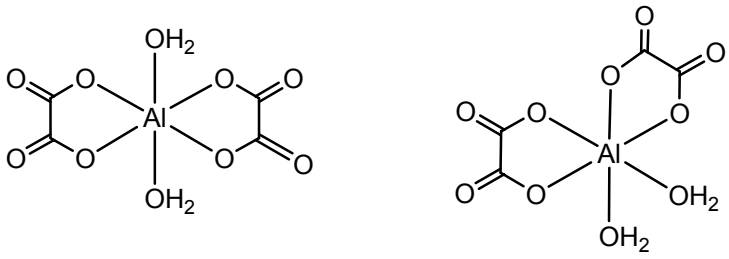

trans *cis*

Figure 33 *trans*- and *cis*-$Al(C_2O_4)_2^-$(Boder et al., 2003)

Table 8 ^{13}C Chemical shifts (ppm from TMS) of detected binary species(Boder et al., 2003).

Species	Chemical shif (ppm)
$Al(C_2O_4)^+$	168.04
trans-$Al(C_2O_4)_2^-$	168.10
cis-$Al(C_2O_4)_2^-$	168.16
$Al(C_2O_4)_3^{3-}$	168.26

Taura (1988) showed that the ^{13}C-NMR signals of the coordinated carboxylates were markedly shifted downfield in protic solvents in comparision with aprotic solvents because the $[Co(edta)]^-$ anion interacts with solvent molecules through the hydrogen bonding between solvent hydrogens and carboxyl oxygens of the complex anion.The protic sovents that have large the acceptor number (AN) values strongly interact in the outer sphere with the carboxylates of the $[Co(edta)]^-$ anion, and this interaction causes the downfield shifts in protic solvents. The result are summarized in Table 9.

Table 9 Effect of solvent to AN parameter and chemical shift (Taura, 1988)

solvent	AN[a]	δ COO^-(ppm)
H_2O	54.8	183.3
$CHCl_3$	23.1	180.6
DMF	16.0	179.5
DMA	13.6	179.5

[a] The acceptor number (AN) of the solvent as measure of estimating the electrophilic ability of solvents. (Protic solvent that have large AN values strongly interact in outer sphere.)

4.1.2 EPMA/EDX

Generally, EPMA/EDX was used to study the elemental composition of products which peak of each element show at different position as in the XRF method. In this work crystal of products were used in the analyses and the height of peaks reflect the ratio of element in products.

From the experiment, the composition of $K_3Al(C_2O_4)_3 \cdot 3H_2O$, Blue, RedCubic, and AlCubic were determined. As an example, $K_3Al(C_2O_4)_3 \cdot 3H_2O$ consists of K, Al, C, and O and the height of peaks were related with general formula in Table 6. Similarly, the ratio of elemental composition (from the height of peaks) in Blue and $K_3Al(C_2O_4)_3 \cdot 3H_2O$ are similar but Blue has the Cr impurity. RedCubic and AlCubic can also be concluded to have the same composition, by the same approach, but RedCubic has the Cr impurity in agreement with the general formula in Table 6.

4.1.3 XRD Pattern

The XRD patterns of the Blue and $K_3Al(C_2O_4)_3 \cdot 3H_2O$ are shown for comparison in Figure17. Both patterns are similar implying they are isomorphous but it should be borne in mind that Blue has a small amount of Cr in the crystal structure. Same as the XRD patterns of RedCubic and AlCubic that are shown in Figure 18, the same can be said that both patterns are similar implying isomorphology and that the RedCubic has a small amount of Cr.

The above conclusion can be supported by the work of Del Arco et al.(2003), where the similarity of the XRD patterns of precursor and product were reported. The powder XRD patterns for samples MgAlCrR and MgAlCrI, together with those of the corresponding precursors (MgAlC and MgAlN), are shown in Figure 34. The PXRD pattern for sample MgAlCrRH (not shown) is similar to that from sample MgAlCrR, although the diffraction maxima are stronger.(Del Arco et al., 2003)

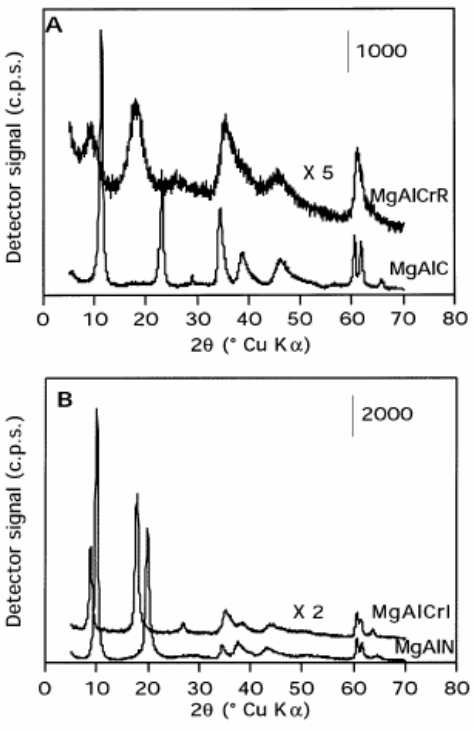

Figure 34 Powder X-ray diffraction patterns of (A) sample MgAlCrR and precursor MgAlC, and(B) sample MgAlCrI and sample MgAlN(Del Arco et al., 2003)

4.1.4 Density of crystal

Density of RedCubic was determined in this work to be 1.92 Mg/m^3. However, the densities of RedHexagonal and Blue could not be determined since their densities appeared to be higher than the solution available for this measurment. Therefore, we concluded that their densities must be higher than that of RedCubic.

Since the structure of RedHexagonal could be solved (in Laongjit's work) so we tried to calculate its density from single crystal X-ray data which came out to be 2.074 Mg/m^3. This figure confirmed our conclusion above that the density of the RedHexagonal should be higher than that of the RedCubic.

4.1.5 Single crystal X-ray diffraction

Cell parameters of the Blue are similar to $K_3[Al(C_2O_4)_3]\cdot 3H_2O$, $K_3[Cr(C_2O_4)_3]\cdot 3H_2O$ and $K_3[Fe(C_2O_4)_3]\cdot 3H_2O$ which are isomorphous (Fenn et al., 1967) and cell parameters of RedCubic are similar to AlCubic (Table 10). Consequently, Blue, $K_3[Al(C_2O_4)_3]\cdot 3H_2O$, $K_3[Cr(C_2O_4)_3]\cdot 3H_2O$, $K_3[V(C_2O_4)_3]\cdot 3H_2O$, and $K_3[Fe(C_2O_4)_3]\cdot 3H_2O$ are isomorphous and so are the RedCubic and AlCubic. This agree with general formula in Table 6.

Table 10 Cell parameter of products and other oxalato complexes

Sample	Unit cell dimensions					
	a(Å)	b(Å)	c(Å)	$\alpha(^\circ)$	$\beta(^\circ)$	$\gamma(^\circ)$
$K_3[Al(C_2O_4)_3]\cdot 3H_2O$ (Taylor, 1978)	7.712	19.518	10.286	90	108.21	90
$K_3[Cr(C_2O_4)_3]\cdot 3H_2O$ (Taylor, 1978)	7.714	19.687	10.361	90	108.06	90
$K_3[Fe(C_2O_4)_3]\cdot 3H_2O$ (Delgado, 2002)	7.762	19.937	10.353	90	107.75	90
$K_3[V(C_2O_4)_3]\cdot 3H_2O$ (Fenn et al., 1967)	7.81	20.01	10.35	90	108.33	90
Blue5%	7.682	19.431	10.215	90	108.11	90
RedCubic5%	20.999	20.999	20.999	90	90	90
AlCubic	20.96	20.964	20.966	90	90	90

4.1.6 UV-Vis spectroscopy

In this work, spectra of products were studied and compared with precursors. The spectra were acquired in solution and solid state: aqueouse solution, solid state (powder and crystalline). UV-Vis spectra of $K_3[Al(C_2O_4)_3]\cdot 3H_2O$, $K_2C_2O_4$, and $H_2C_2O_4$ in this work show absorption band of oxalate anion with the same position at 293 nm in aqueous solution and a marked shoulder on band of high intensity, which extends into the far ultra-violet at 253 nm in powder form

The absorption spectra of aqueous solutions of oxalic acid and potassium oxalate and of methyl oxalate in hexane were determined, a band of low intensity at a wavelength of about 250 nm appeared as a marked shoulder on band of high intensity, which extends into the far ultra-violet. This low intensity band did not appear in the absorption of potassium oxalate, but were observed as an inflexion in the absorption curve of oxalic acid (Figure 35) (Graddon, 1956).

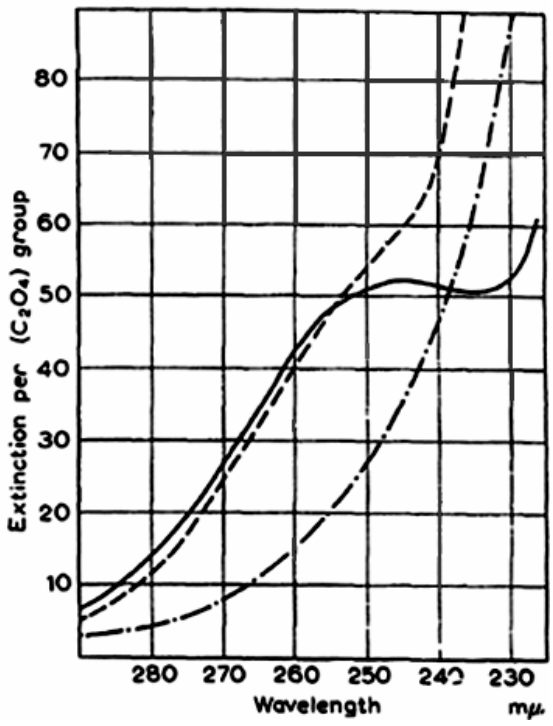

Figure 35 Absorption spectra of oxalic acid(----), potassium oxalate(-·-·-·-·), methyl oxalate(____) (Graddon, 1956)

The appearance of a band in the region 210-260 nm is characteristic of the covalently bound carboxylic group and probably represents transition of the π-electrons of the carbonyl group, transition which do not occur in the carboxylate ion owing to the equivalence of the oxygen atoms. (Graddon, 1956)

[However, the different nature of carboxyl groups is also shown in the infra-red region,particularly in the C=O stretching fundamentals in the region 1600-1750 cm^{-1} which normally occur with a frequency in the region 1700-1750 cm^{-1} for esters of carboxylic acid and in the region 1600-1650 cm^{-1} for their salt, a clear distinction being observed between carboxyl groups linked to neighbouring atom by covalent and ionic bonds.(Graddon, 1956)]

In general, there are three types of absorption curve characteristic of oxalic acid or its simple derivatives: (Graddon, 1956)

1. A band of low intensity about 250 nm appearing as a shoulder on a band of high intensity extending into the far ultra-violet,observed in methyl oxalate and molecular oxalic acid, that is in molecules in which the carboxyl group is covalently bound.
2. A high-intensity absorption in the far ultra-violet without accompanying low intensity band, characteristic of the oxalate ion, $(C_2O_4)^{2-}$.
3. An absorption curve with an inflexion about 250 nm, probably due to masking of the low-intensity band by a shift or broadening of the high-intensity band: characteristic of the $(HC_2O_4)^-$ ion in which one carboxyl group only is covalently bound to hydrogen.

In this work, Redcubic, RedHexagonal, Blue, and $K_3[Cr(C_2O_4)_3]\cdot 3H_2O$ show the strong absorption band of oxalate anion with the same position at 293 nm in aqueous solution assigned to the $\pi \rightarrow \pi^*$ electronic transition. This is similar to that observed when $K_3[Al(C_2O_4)_3]\cdot 3H_2O$, $K_2C_2O_4$, and $H_2C_2O_4$ dissolved in water where they appeared to appreciably dissociated into ions and showed absorption at wavelengths longer than 250 nm. In powder form, these complexes showed a marked shoulder on band of high intensity, which extends into the far ultra-violet in region 256-273 nm similar to that observed in other oxalato complexes studied by Graddon as shown in Figure 36.

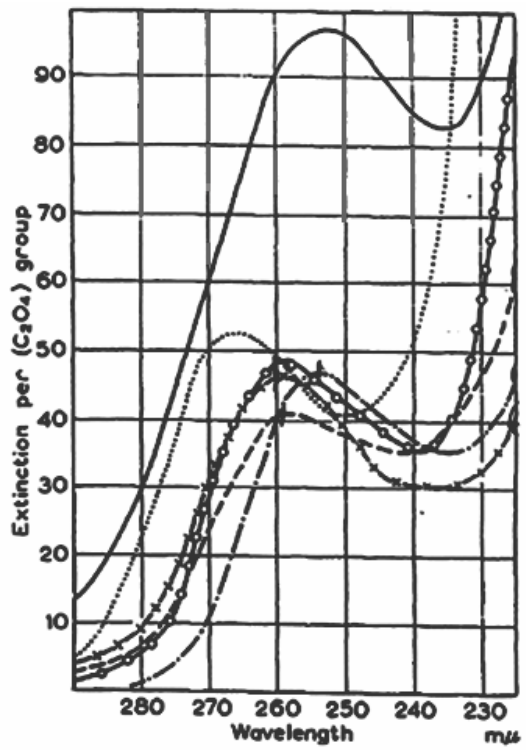

Figure 36 Spectra of oxalate in other oxalato complexes(---)Be, (-.-.)Mg, (-x-x)Al, (.....)Zr, (-o-o)Th, and (_____)Cu (Graddon, 1956)

Absorption spectra of oxalato complexes of beryllium, aluminium, zirconium, magnesium, copper, and thorium (Figure 36) by Graddon (1956) showed a low intensity band appearing in the region 250-270 nm. This low intensity band appeared to be displaced to longer wavelengths by co-cordination of the oxalate group to a metal cation; the extent of displacement depending upon the size and valency of cation.

Absorption band of Redcubic, RedHexagonal, Blue, and $K_3[Cr(C_2O_4)_3]\cdot 3H_2O$ are in agreement with $K_3[Al(C_2O_4)_3]\cdot 3H_2O$, $K_2C_2O_4$, and $H_2C_2O_4$ where the absorption band at 250-270 nm in solid state and at 293 nm in aqueous solution can be assigned to an internal transition ($\pi \rightarrow \pi^*$) within the oxalate group. This also agrees with the work of Cindric´ (2000) who studied the UV spectra of $[Mo_2O_5(C_2O_4)_2(H_2O)_2]$ and $M_2[MoO_3(C_2O_4)]\cdot H_2O$ (M=Na, K, Rb, Cs) complexes in aqueous solutions showing an internal transition within the oxalate group at *ca*.285 nm (35000 cm^{-1}), but rather weak.

For chromium (III) complexes, assuming a cubic octahedral field to be present, the electronic ground state will be a $^4A_{2g}$ state arising from the strong-field configuration $(t_{2g})^3$. Other states springing from this configuration are ^2E_g, $^2T_{1g}$, and $^2T_{2g}$. The next strong-field configuration is $(t_{2g})^2(e_g)$, producing the quartet state $^4T_{2g}$ and $^4T_{1g}$ (Ballhausen, 1962). Those states are shown in Tanabe Sugano diagram (Figure 37) which is able to predict the transition energies for both spin-allowed and spin-forbidden transitions, as well as for both strong field (low spin), and weak field (high spin) complexes. The spin-allowed transition are $^4A_{2g} \rightarrow {}^4T_{2g}$, $^4A_{2g} \rightarrow {}^4T_{1g}$ (F), and $^4A_{2g} \rightarrow {}^4T_{1g}$(P), while the spin-forbidden transitions are $^4A_{2g} \rightarrow {}^2E_{2g}$, $^2T_{1g}$ and $^4A_{2g} \rightarrow {}^2T_{2g}$.

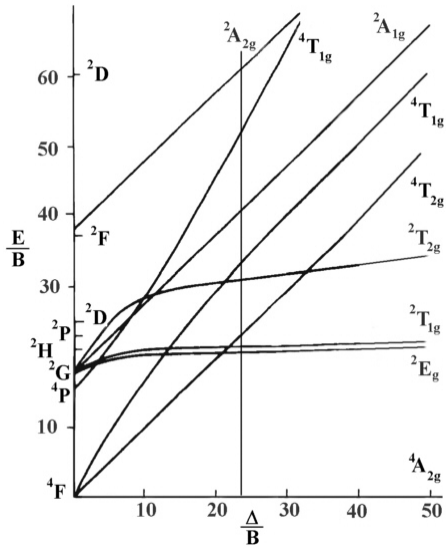

Figure 37 Tanabe-sugano diagram for d^3 octahedral complexes (Cotton and Wilkinson, 1972)

The simplified Orgel diagram (Figure 38) is useful for showing the energy levels of both high spin octahedral and tetrahedral transition metal ions. They only show the spin-allowed transitions. three absorptions of Cr oxalato complexes are expected. In practice, the spectrum is found to contain 3 bands which occur at 17,500 cm^{-1}, 24,000 cm^{-1} and 38,100 cm^{-1}(571 nm, 416 nm, and 262 nm). Interpreting these as the transitions $^4A_{2g} \rightarrow {}^4T_{2g}$, $^4A_{2g} \rightarrow {}^4T_{1g}$ (F), and $^4A_{2g} \rightarrow {}^4T_{1g}$(P). In general, only two are observed, the third band usually is not experimentally observed because it is masked by the charge transfer spectrum.(Huheey et al., 1993)

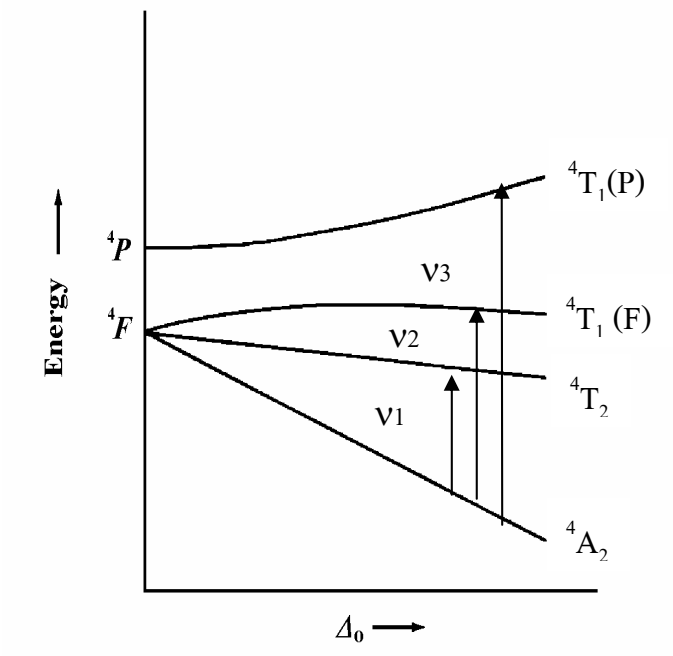

Figure 38 Orgel diagram of Cr(III) (Huheey et al., 1993)

In aqueous solution, RedCubic, RedHexagonal, Blue, and $K_3[Cr(C_2O_4)_3]\cdot 3H_2O$ show the same greenish purple color. The absorption spectra of all products (in this work) in aqueous solution were very similar to that of $[Cr(C_2O_4)_3]^{3-}$ ion which showed three bands at about 420($^4A_{2g} \rightarrow {}^4T_{1g}$ (F)), 570($^4A_{2g} \rightarrow {}^4T_{2g}$), and 698 nm ($^4A_{2g} \rightarrow {}^2E_{2g}$, $^2T_{1g}$) (Yager T.D., 1979). All of these spectra showed the first two spin-allowed bands appearing at about 422 and 574 nm virtually the same pattern as found in other chromiun oxalato complexes compiled in Table 11.

Table 11 Visible absorption maxima for Cr (III) complexes in aqueous solution

Compound	$^4A_{2g} \rightarrow {}^4T_{1g}$(F) (nm)	$^4A_{2g} \rightarrow {}^4T_{2g}$ (nm)
$K_3[Cr(C_2O_4)_3]\cdot 3H_2O$[a]	420	570
$K[Cr(ox)_2phen]\cdot 4H_2O$[a]	397	543
$K[Cr(ox)_2bipy]\cdot 3H_2O$[a]	392	535
trans-K $[Cr(H_2O)_2(C_2O_4)_2]\cdot 3H_2O$[b]	416	555
cis-K $[Cr(H_2O)_2(C_2O_4)_2]\cdot 3H_2O$[b]	416	562

[a]Broomhead et al., 1968, [b]Cunningham et al., 1952

In powder form (Figure 23), RedCubic, RedHexagonal, Blue, and $K_3[Cr(C_2O_4)_3]\cdot 3H_2O$ have different colors and show slightly different absorption peaks. Their spectra show similar pattern to that in aqueous solution. However, on a closer inspection, there are two interesting points, showing slight differrences as shown in Figure 39. The first one, point (A), the trough in the spectra of Blue and $K_3[Cr(C_2O_4)_3]\cdot 3H_2O$ occur at 493 nm but in RedCubic and RedHexagonal occur at 482 nm. The other, point(B), the transition $^4A_{2g} \rightarrow {}^4T_{2g}$ of RedCubic in powder forms are observed at 571 nm while that of Blue appear at 580 nm. These differences will help to explain the different colors of these products. The relations between the wavelength ranges and colors in the visible spectrum are shown in Figure 40.

The absorption patterns observed in this work agree with the work of Tamaki et al. (1992) when they observed the powder reflectance spectra of $\{NBu_4[MCr(C_2O_4)_3]\}_x$(M= Mn^{2+}, Co^{2+}, Ni^{2+}, Cu^{2+}, and Zn^{2+}). Their spectra showed three d-d band characteristic of $[Cr(C_2O_4)_3]^{3-}$(420, 580, and 698 nm) which they explained that the inert chromium (III) ion retained the original six-coordinate environment with three oxalate group.

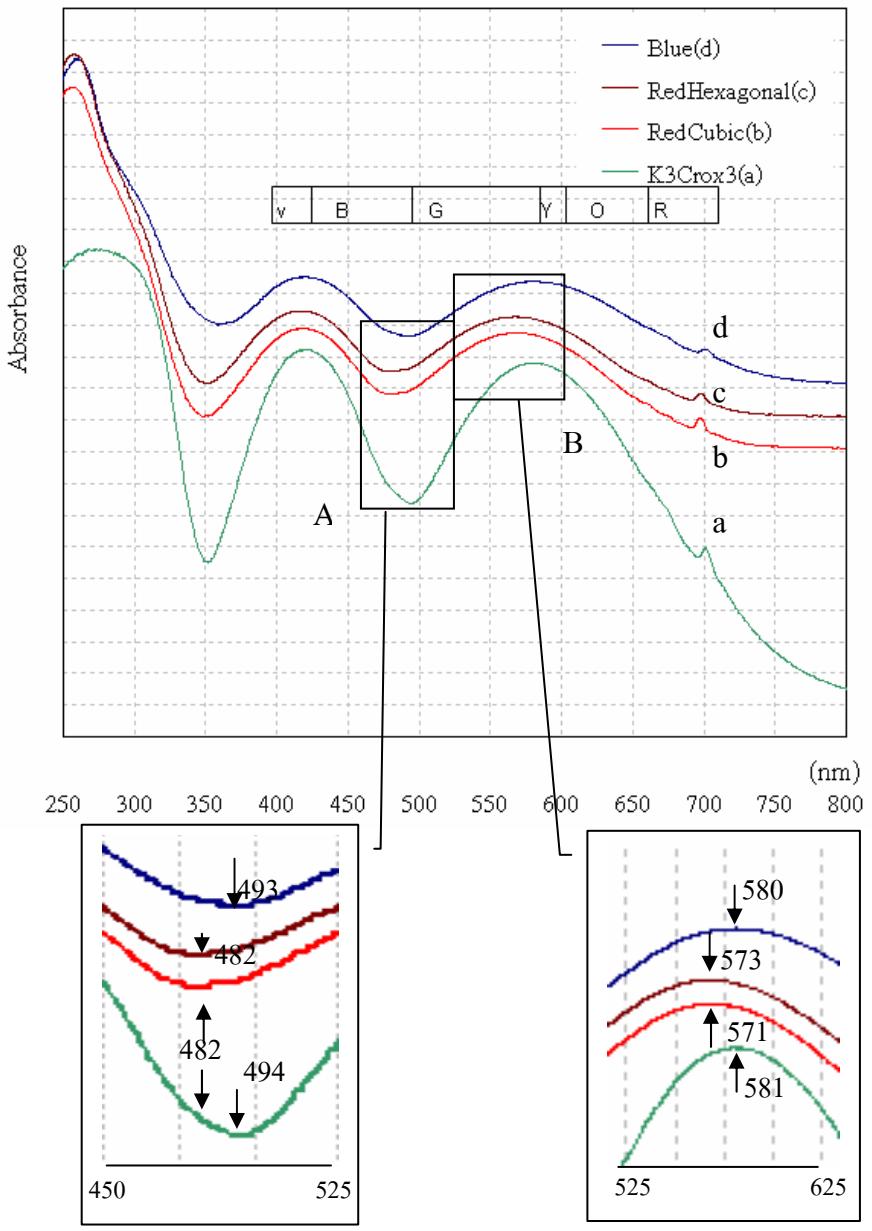

Figure 39 UV-Visible absorption spectra of RedCubic, Blue, RedHexagonal, and $K_3Cr(C_2O_4)_3 \cdot 3H_2O$ in powder form by diffused reflectance method

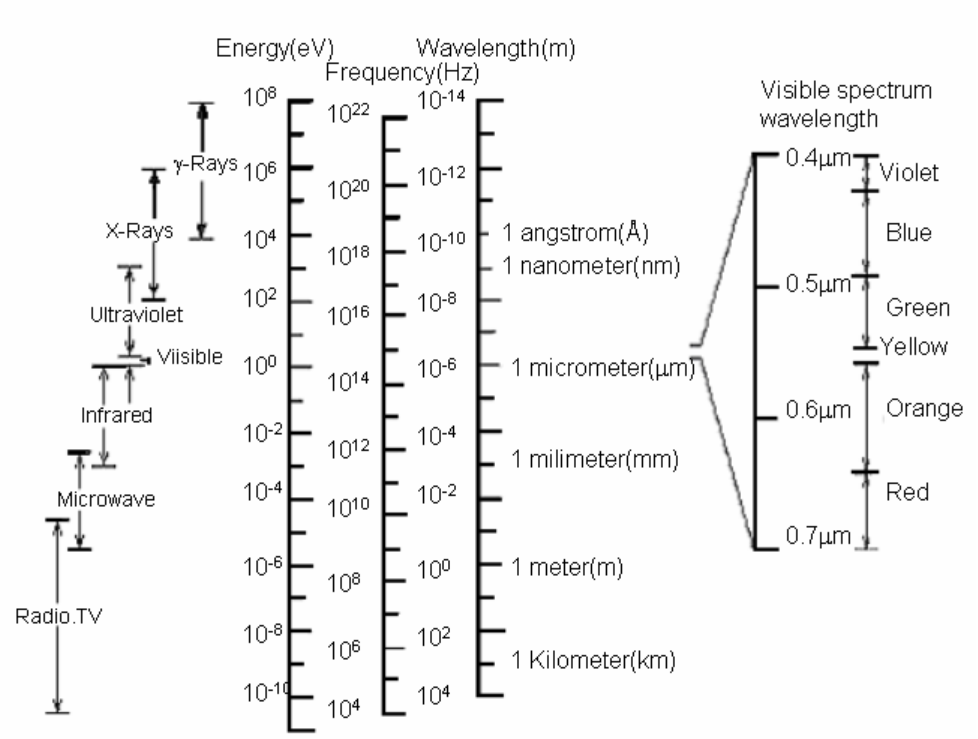

Figure 40 The spectrum of electromagnetic radiation, including wavelength ranges for the various colors in the visible spectrum. (www.chemistry.ohio-state.edu)

In the spectra of crystalline (Figure 24), RedCubic and Blue showed absorption bands $^4A_{2g} \rightarrow {}^4T_{1g}$ (F), $^4A_{2g} \rightarrow {}^4T_{2g}$ and $^4A_{2g} \rightarrow {}^2E_{2g}$, $^2T_{1g}$ of $[Cr(C_2O_4)_3]^{3-}$ ion which are obviously different as shown in Table 5. The results are similar to those from powder form. However, in aqueous solution both compounds showed similar absorption bands.

Similary, Decurtins et al., 1994 reported that the polarized single crystal absorption spectra of $[Cr(C_2O_4)_3]^{3-}$ doped into $NaMg[Al(C_2O_4)_3]$ corresponding to the $^4A_{2g} \rightarrow {}^4T_{2g}$ and the $^4A_{2g} \rightarrow {}^4T_{1g}$ transition were centered at 568 and 424 nm, respectively.

Schönherr et al. (1989) reported the absorption band of 1%Cr^{3+} doped in $NaMg[Al(C_2O_4)_3]\cdot 8H_2O$ at T= 90 K which is shown in Figure 41.

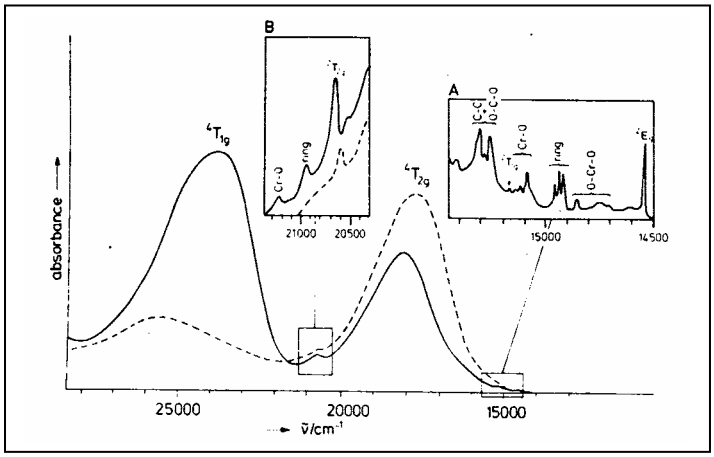

Figure 41 Absorption spectrum of 1% Cr^{3+} doped in $NaMg[Al(C_2O_4)_3]\cdot 8H_2O$ at T=90K (Schönherr et al., 1989)

Figure 42 shows the two spin allowed transitions for Cr^{3+} in ruby give rise to absorption in the violet and the green. Since the transmission in the red is much more than the transmission in the blue so rubies are red. The $^2E \rightarrow {}^4A_2$ fluorescence adds to the deep red color of a ruby. On the other hand, Figure 43 shows the transitions for Cr^{3+} in beryl. The crystal field splitting is a little bit smaller than ruby, so that the lower energy absorption is shifted to lower energy taking out much of the reflectance of red light and changing the color to green.

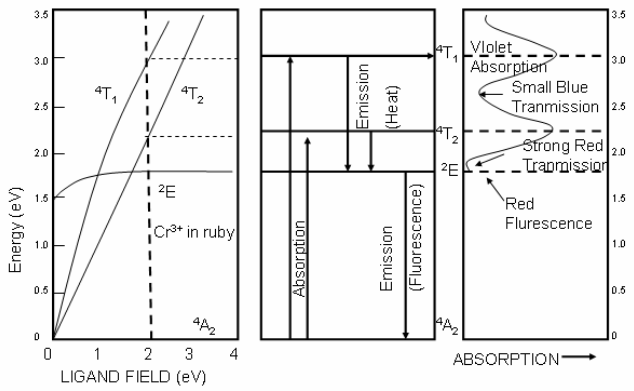

Figure 42 Absorption spectrum of ruby (www.chemistry.ohio-state.edu)

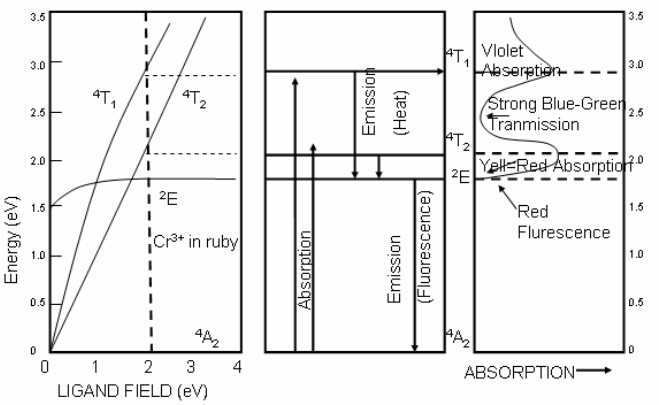

Figure 43 Absorption spectrum of beryl (www.chemistry.ohio-state.edu)

One more evidence can confirm different colour of products in this work when we viewed UV-Vis in powder and crystalline. In RedCubic, the transmission of the red color is much more than that in the blue (Figure 44). This results agree with the difference of color between RedCubic and Blue in powder and crystalline.

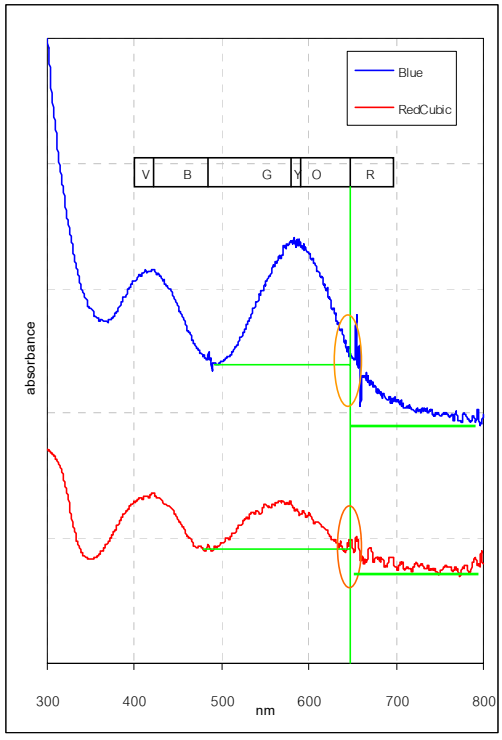

Figure 44 UV-Visible absorption spectra of RedCubic, and Blue crystalline

In this work, not only the main peaks are found in UV-Vis spectrum but also there is a very small peak due to spin-forbidden that show clearly at 699 and 655 nm for powder and crystalline, respectively. It can be assigned to the transition $^4A_{2g} \rightarrow {}^2E_{2g}, {}^2T_{1g}$

About spin-forbidden transitions, it is well known that the spectra of bulk ruby (chromium-doped α-Al_2O_3) single crystals contain two sharp lines at 694.3 and 692.9 nm (R1 and R2-lines at room temperature), which are due to emission from isolated Cr^{3+} ions substituted at Al sites. The ground state of Cr^{3+} is then $^4A_2$, while the first excited state is ^2E. The transition involved is the spin forbidden $^2E \rightarrow {}^4A_2$ transition within the d^3 configuration of the Cr^{3+} ions subject to the crystal field of the surrounding oxygen ligands. According to the diagram of Tanabe and Sugano, the ^2E excited state is weakly affected by the crystal field, and the $^2E \rightarrow {}^4A_2$ transition is a sharp zero phonon doublets split by the combined action of the spin–orbit coupling and the small trigonal component of the full crystal field. Like most complexes of Cr (III), the oxalato complexes, with a variety of counterions, display a distinctive emission at low temperatures, such as liquid nitrogen (77K). In the oxalate complexes, this emission is dominated by two sharp lines and is assigned as arising from the transition $^2E \rightarrow {}^4A_2$. In the complex $K_3Al(C_2O_4)_3$ the two sharp line mentioned above are separated by 82 cm^{-1} and occur at 688.94 and 692.38 nm. The splitting is due to a splitting of the ^2E state caused by a spin-orbit interaction. (Coleman, 1982)

The color in RedCubic and RedHexagonal are similar to ruby. The deep red color of ruby results from the substitution of a small number of chromium atom“impurities” into an aluminum oxide (corundum) crystal. Because Cr^{+3} has the valence–electron configuration $3d^3$, its ground state in the octahedral site in the crystal has all three electrons with spins parallel in the lower–energy t_{2g} levels. When light of the proper wavelength shines on such an ion, either one or two of these electrons can be excited into the higher–energy e_g level, giving rise to two strong absorption bands in the

visible region of the spectrum. The lower–energy band causes the absorption of green and yellow light and the other the absorption of violet light. The two bands overlap, so that most of the blue light is also absorbed, but some passes through and combines with the strongly transmitted red light to give the characteristic slightly purplish red of the ruby. Orgel (1957) studied on "Ion compression and the color of ruby" and found that the red color that should have been green, of ruby was due to an absorption band the maximum of which was 19,000cm^{-1} (526nm). Thus, according to his interpretation, the crystal field parameter Δ in ruby has increased by 20 percent relative to that in other oxide materials. In the electrostatic theory, Δ is proportional to R^{-5} where R is the metal-anion distance, so that a reduction of 20 percent in Δ corresponds to a reduction of metal-oxygen distance by 4 percent. Taking the radius of the chromium ion as 0.65 A and that of the oxygen ion as 1.40A, he found a normal Cr-O distance distance of 2.05 A, so that a shortening of the the Cr-O distance by 0.08 A would be sufficient to account for the observed difference in color (Orgel, 1957).

Ballhausen (1962) reported that the absorption spectrum of ruby (Cr^{3+}, Al_2O_3) showed two broad band at 400, and 556 nm corresponding the $^4A_{2g} \rightarrow {}^4T_{2g}$ and the $^4A_{2g} \rightarrow {}^4T_{1g}$ transition.

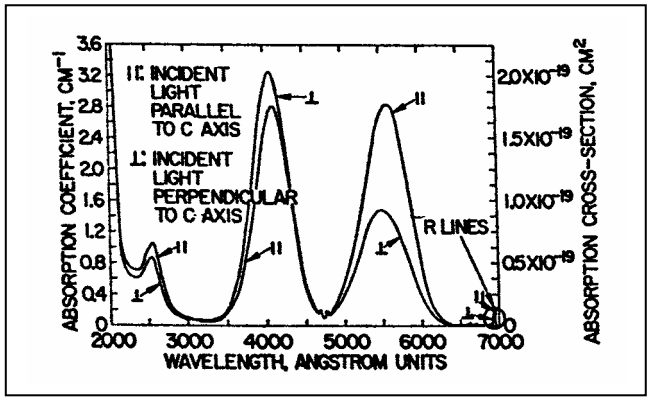

Figure 45 Absorption spectrum of ruby (Maiman, 1961)

In addition, RedCubic and RedHexagonal show alexandrite effect which was the color-change property under different light sources (fluorescence and incandescence lights). In this case, the largest valley (transmission window = low in the absorption graph) occurs at the red end of the spectrum, thus the product essentially looks red. (However, a smaller transmission window may occur at blue wavelengths. This gives a purplish cast to the red color of them).

The "Alexandrite" color change effect:

Color change due to change in the color of incident light (recall that fluorescent light is bluish (rich in blue wavelengths) and candle light is rich in red and orange wavelenghts). Alexandrite is the best known example of a gemstone that changes color depending upon the light it is viewed under.

In the case of alexandrite, there are two approximately equal sized tranmission windows - the first at blue and second at red wavelengths. When viewed in light made up of all wavelenghts, the stone tramsmits blue and red and often looks purple or purple-grey. The results were shown in Figure 46. (www.socrates.berkeley.edu)

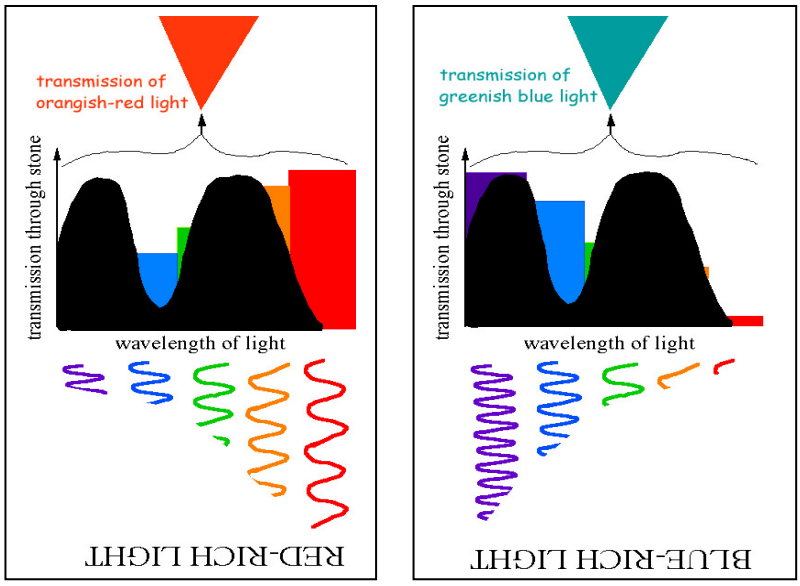

Figure 46 Pictures of alexandrite effect.(www.socrates.berkeley.edu)

Suchocki et al., 1987 studied “Spectroscopic properties of alexandrite crystals”. Alexandrite ($BeAl_2O_4$:Cr^{3+}) has Cr^{3+} ions occupying the Al^{3+}lattice sites. The two broad band are associated with transition to the $^4T_{1g}$ and $^4T_{2g}$levels, while the shoulder on the band edge near 245 nm may either be due to a charge tranfer transition or to a transition terminating on one of the higher levels of the $3d^3$configuration such as the $^4T_{1g}$(P) levels. At low temperatures,the sharp line appearing on the low-energy side of the $^4T_{2g}$ band between about 580 and 670 nm include zero-phonon transitions to components of the $^2T_{1g}$ and $^4T_{2g}$ level, and phonon peaks in the vibronic side bands of both the R_{1m} line and the$^4T_{2g}$ zero-phonon lines (Figure 47).

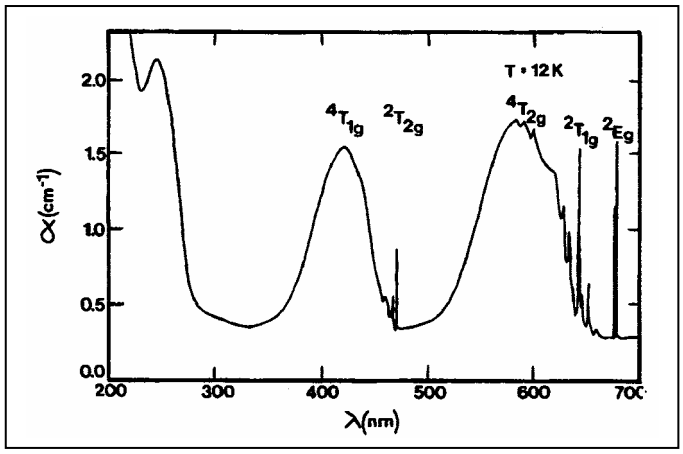

Figure 47 Electronic absorption spectrum of alexandrite($BeAl_2O_4$:Cr^{3+}) (Suchocki, 1987)

According to data from elemental analysis, RedCubic and Blue contain different cations and appear as different color (reddish purple, and Blue, respectively). Therefore, different cation may associate with compression in structure (metal-ligand distance) and is the cause for the color difference in these products.

Another evidence that support the effect of surrounding arrangement on the electronic absorption spectrum came from the work of Ameis et al., 1985 where they studied Jahn-Teller effect of Ti^{3+} in octahedral coordination of of $A_2A'TiCl_6$ for A, A'= Cs, K, and Rb, Na, respectively. They found that a small static tetragonal compression of the $TiCl_6^{2-}$ octahedral due to geometric packing forces is present below the phase transition (Figure 48).

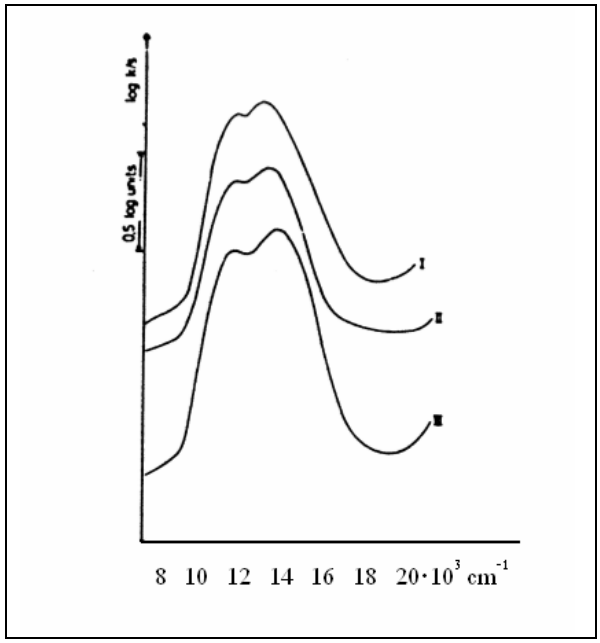

Figure 48 Electronic absorption spectrum of $Rb_2NaTiCl_6$(I), Cs_2KTiCl_6(II), and Rb_3TiCl_6(III) (Ameis et al., 1985)

Whereas Coleman et al., 1975 studied about environmental effects on the $^2E \rightarrow {}^4A_2$ luminescence of a series of Cr (III)-oxalate complexes. The phosphorescence of the $Cr(C_2O_4)_3^{3-}$ ion had been studied in 13 crystal lattices. The results obtained were quite distinctively different in each environment.

4.2 Characterization of products obtained by varying % Cr

From the original Laongjit's method, products were prepared by mixing $K_3Al(C_2O_4)_3 \cdot 3H_2O$, $K_3Cr(C_2O_4)_3 \cdot 3H_2O$, and NaCl in a given ratio resulting in mixture of three types of products which was difficult to isolate from each other. New method was needed to yield only one type of product such as Blue and RedCubic as shown in Figures 27-30. When added excess NaCl (1.688g) to the mixed solution of $K_3Al(C_2O_4)_3 \cdot 3H_2O$ and, $K_3Cr(C_2O_4)_3 \cdot 3H_2O$, only RedCubic crystal was obtained. Furthermore, if small amount of $Pr_6O_{11}$was added only Blue crystal was obtained. Products obtained from these new methods were essentially identical to those obtained by Laongjit's method .

Products with varying %Cr were then prepared and their elemental compositions were determined by ICP-AES and WDXRF. The results showed that %K and %Na were rather constant but %Al decreased as %Cr was increased (Figures 27-30). In addition, when %Cr increased the color became darker (Figure 25). This could be viewed as the displacement of chromium atoms at aluminium sites in the molecule of products and the color intensity varied with the chromiun concentration.